Linear dielectric response of clustered living cells

Titus Sandu,[1] Daniel Vrinceanu,[2] and Eugen Gheorghiu[1,*]
[1]*International Center for Biodynamics, Bucharest, Romania*
[2]*Department of Physics, Texas Southern University, Houston, Texas 77004, USA*
(Received 11 September 2009; revised manuscript received 13 January 2010; published 11 February 2010)

The dielectric behavior of a linear cluster of two or more living cells connected by tight junctions is analyzed using a spectral method. The polarizability of this system is obtained as an expansion over the eigenmodes of the linear response operator, showing a clear separation of geometry from electric parameters. The eigenmode with the second largest eigenvalue dominates the expansion as the junction between particles tightens, but only when the applied field is aligned with the cluster axis. This effect explains a distinct low-frequency relaxation observed in the impedance spectrum of a suspension of linear clusters.

DOI: 10.1103/PhysRevE.81.021913 PACS number(s): 87.19.rf, 87.50.C−, 41.20.Cv

I. INTRODUCTION

Particle polarizability governs the electric response for many inhomogeneous systems ranging from biological cells to plasmonic nanoparticles and depends strongly on both its dielectric and geometric properties. Analytical models have been reported [1,2] only for spherical and ellipsoidal geometries, whereas more complex geometries have been approached by direct numerical solution of the field equations using, for example, the finite difference methods [3], the finite element method [4], the boundary element method [5,6], or the boundary integral equation (BIE) [7].

In a simplified representation, biological cells can be regarded as homogeneous particles (cores) covered by thin membranes (shells) of contrasting electric conductivities and permittivities. Complex geometries occur when cells are undergoing division cycles (e.g., budding yeasts) or are coupled in functional tissues (e.g., lining epithelia or myocardial syncytia). In these cases, the dielectric/impedance analysis of cellular systems is far more complicated than previous models [8–10], which considered suspensions of spherical particles. Intriguing dielectric spectra [11] reveal distinct dielectric dispersions with time evolutions consistently related to tissue functioning or alteration, identifying a possible role in cell connectors (gap junctions) in shaping the overall dielectric response.

A direct relation between the microscopic parameters and experimental data can be analytically derived only for dilute suspensions of particles of simple shapes, and is rather challenging for system with more realistic shapes, where only purely numerical solutions have been available. In this work, we demonstrate that a spectral representation of a BIE provides the analytical structure for the polarizability of particles with a wide range of shapes and structures. The numerically calculated parameters encode particle's geometry information and are accessible by experiments.

By using single and double-layer potentials [12], the Laplace equation for the fields inside and outside the particle is transformed into an integral equation. A spectral representation for the solution of this equation is obtained providing the eigenvalue problem for the linear response operator is solved. Although not symmetric, this operator has a real spectrum bounded by $-1/2$ and $1/2$ [13–15] and its eigenvectors are orthogonal to those of the conjugate double-layer operator. A matrix representation is obtained by using a finite basis of surface functions.

The true advantage of the spectral method is that the eigenvalues and eigenvectors of the integral operator provide valuable insight into the dielectric behavior of clusters of biological cells. The eigenvectors are a measure of surface charge distributions due to a field. Only eigenvectors with a nonzero dipole moment contribute to the polarizability of the particle. We call these dipole-active eigenmodes. An effective separation of the geometric and morphologic properties from dielectric properties is therefore achieved [16]. We also show that for a particle covered by multiple confocal shells, the relaxation spectrum is a sum of Debye terms with the number of relaxations equal to the number of interfaces times the number of dipole-active eigenvalues. This is a generalization of a previous result [17] on cells of arbitrary shape.

Our method is related to another spectral approach which uses an eigenvalue differential equation [18–21]. This method has been applied to biological problems by Lei *et al.* [22] and by Huang *et al.* [23]. These authors, however, considered homogeneous cells with much simpler expression for cell polarizability. The BIE spectral method seeks a solution on the boundary surface defining the particle, as opposed to the eigenvalue differential equation, where the solution is defined in the entire space.

In a previous study on double (budding) cells it was shown that before cells separation an additional dispersion occurs [24]. Moreover, in recent papers [3,25] numerical experiments have shown that the dielectric spectra of a suspension of dimer cells connected by tight junctions exhibit an additional, distinct low-frequency relaxation. Our numerical calculation shows that the largest dipole-active eigenvalue approaches the value of 1/2 as the junction become tighter. Although the coupling of this eigenmode with the electric field stimulus is relatively modest (the coupling weight is about 1%–2%), this eigenmode has a significant contribution to the polarizability of clusters. Thus, the eigenmodes close to 1/2 induce an additional low-frequency relaxation in the dielectric spectra of clustered biological cells even though

*egheorghiu@biodyn.ro

the coupling is quite small. Needlelike objects, such as elongated spheroids or long cylinders, have similar polarizability features.

In this paper, we consider rotationally symmetric linear clusters made of up to 4 identical particles covered by thin insulating membranes and connected by junctions of variable tightness. Convenient and flexible representations for the surfaces describing these objects are provided. The number of relaxations in the dielectric spectrum of the linear clusters, their time constants and their relative strengths are analyzed in terms of the eigenmodes of the linear response operator specific to the given shape.

II. THEORY

A. Effective permittivity of a suspension

We consider a suspension of identical, randomly oriented particles of arbitrary shape and dielectric permittivity, ε_1, immersed in a dielectric medium of dielectric permittivity, ε_0. The dielectric permittivities are in general complex quantities and the theory described here applies also for time-dependent fields, providing that the size of a particle is much smaller than the wavelength. When an applied uniform electric field interacts with the suspension, the response of the system is linear with the applied field and an effective permittivity for the whole sample can be measured and is defined by [25–27],

$$\varepsilon_{\text{sus}} = \varepsilon_0 + f\frac{\alpha\varepsilon_0}{1 - f\frac{\alpha}{3}}. \tag{1}$$

This result is obtained in the limit of low concentration, weak intensity of the stimulus field, and using an effective medium theory within the dipole approximation. Here, $f = NV_1/V$ is the volume fraction of all N particles, each of volume V_1, with respect to the total volume of the suspension V. The averaged normalized polarizability α of a particle is defined as [25,27,28]

$$\alpha = \frac{1}{4\pi V_1}\int_{V_1}\int_{\Omega_N}\left(\frac{\varepsilon_1 - \varepsilon_0}{\varepsilon_0}\right)\mathbf{E}(\mathbf{N})\cdot\mathbf{N}d\Omega_N dV, \tag{2}$$

where $\mathbf{E}(\mathbf{N})$ is the electric field perturbation created inside the particle under a normalized applied electric excitation with direction $\mathbf{N}$ and $d\Omega_N$ is the solid angle element generated by that direction. The above normalized polarizability is dimensionless and is obtained by multiplying the standard polarizability of a particle with the factor $4\pi/V_1$. In the following, we will refer only to normalized polarizability, thus, without any confusion, the normalized polarizability α will be simply called polarizability. The directional average in Eq. (2) is equivalent to the mean value of polarizabilities along any three orthogonal axes because the problem is linear with respect to the applied field. In order to calculate the effective permittivity, it is therefore enough to obtained polarizabilities for three directions of the field and use their mean value.

The electric field inside a particle is obtained by solving the following Laplace equation for the electric potential Φ:

$$\Delta\Phi(\mathbf{x}) = 0, \quad \mathbf{x} \in \Re^3 \setminus \Sigma,$$

$$\Phi|_+ = \Phi|_-, \quad \mathbf{x} \in \Sigma$$

$$\varepsilon_0 \frac{\partial\Phi}{\partial\mathbf{n}}\bigg|_+ = \varepsilon_1 \frac{\partial\Phi}{\partial\mathbf{n}}\bigg|_-, \quad \mathbf{x} \in \Sigma,$$

$$\Phi \to -\mathbf{x}\cdot\mathbf{N}, \quad |\mathbf{x}| \to \infty, \tag{3}$$

where $\Re^3$ is the Euclidian three-dimensional space and Σ is the surface of the particle. The derivatives are taken with respect to the normal vector $\mathbf{n}$ to the surface Σ.

Due to the mismatch between the polarization inside and outside the object, electric charges accumulate at the interface Σ and create an electric potential which counteracts the uniform electric field stimulus. The solution of the above Laplace problem [Eq. (3)] is therefore formally given by

$$\Phi(\mathbf{x}) = -\mathbf{x}\cdot\mathbf{N} + \frac{1}{4\pi}\int_\Sigma \frac{\mu(\mathbf{y})}{|\mathbf{x}-\mathbf{y}|}d\Sigma(y). \tag{4}$$

The single layer charge distribution μ induced by the normalized electric field is a solution of the following BIE, obtained by inserting solution (4) in Eqs. (3)

$$\frac{\mu(\mathbf{x})}{2\lambda} - \frac{1}{4\pi}\int_\Sigma \mu(\mathbf{y})\frac{\mathbf{n}(\mathbf{x})\cdot(\mathbf{x}-\mathbf{y})}{|\mathbf{x}-\mathbf{y}|^3}d\Sigma(\mathbf{y}) = \mathbf{n}(\mathbf{x})\cdot\mathbf{N}. \tag{5}$$

Here, the parameter $\lambda = (\varepsilon_1 - \varepsilon_0)/(\varepsilon_1 + \varepsilon_0)$ isolates all the information regarding the dielectric properties for this problem.

On using the linear response operator M that acts on the Hilbert space of integrable functions on the surface Σ,

$$M[\mu] = \frac{1}{4\pi}\int_\Sigma \mu(\mathbf{y})\frac{\mathbf{n}(\mathbf{x})\cdot(\mathbf{x}-\mathbf{y})}{|\mathbf{x}-\mathbf{y}|^3}d\Sigma(\mathbf{y}), \tag{6}$$

the integral Eq. (5) is written as

$$(1/(2\lambda) - M)\mu = \mathbf{n}\cdot\mathbf{N}. \tag{7}$$

The integral operator (6) is the electric field generated by the single layer charge distribution μ along the normal to the surface. It encodes the geometric information and has several interesting properties [13–15]. Its spectrum is discrete and it is not difficult to show that all of its eigenvalues are bounded by the $[-1/2, 1/2]$ interval. Although nonsymmetric, the operator (6) has real nondegenerate eigenvalues. The eigenvectors are biorthogonal, i.e., they are not orthogonal among themselves, but orthogonal to the eigenvectors of the adjoint operator

$$M^\dagger[\mu] = \frac{1}{4\pi}\int_\Sigma \mu(\mathbf{y})\frac{\mathbf{n}(\mathbf{y})\cdot(\mathbf{x}-\mathbf{y})}{|\mathbf{x}-\mathbf{y}|^3}d\Sigma(\mathbf{y}), \tag{8}$$

which is associated with the electric field generated by a surface distribution of electric dipoles (double-layer charge distribution). Therefore, if $|u_k\rangle$ is a right eigenvector of M corresponding to eigenvalue χ_k, $M|u_k\rangle = \chi_k|u_k\rangle$ and $\langle v_{k'}|$ is a left eigenvector corresponding to eigenvalue $\chi_{k'}$, $\langle v_{k'}|M^\dagger = \chi_{k'}\langle v_{k'}|$, then

$$\langle v_{k'}|u_k\rangle = \delta_{k'k}, \tag{9}$$

with the scalar product defined as the integral over the interface Σ,

$$\langle f_1|f_2\rangle = \int_\Sigma f_1^*(\mathbf{x}) f_2(\mathbf{x}) d\Sigma(\mathbf{x}). \tag{10}$$

The value 1/2 is always the largest eigenvalue of the operator M, regardless the geometry of the object. This is immediately seen if the object is considered to be conductor ($\varepsilon_1 \to \infty$), and then the interior electric field has to be zero. In that case $\lambda = 1$, and the charge density that generates a vanishing internal electric field obeys the equation $(1/2 - M)\mu = 0$, and therefore 1/2 is an eigenvalue of M. However, this eigenmode is not dipole active and does not contribute to the total polarization of the object. The operator (6) is insensitive to a scale transformation, which means that its eigenvalue and eigenvectors depend only on the shape of the object and not on its size, or electrical properties.

By employing the spectral representation of the resolvent of the operator M

$$(z - M)^{-1} = \sum_k (z - \chi_k)^{-1} |u_k\rangle\langle v_k|, \tag{11}$$

the solution of Eq. (7) is obtained for $z = 1/(2\lambda)$ as

$$\mu = \sum_k \langle v_k|\mathbf{n}\cdot\mathbf{N}\rangle (1/(2\lambda) - \chi_k)^{-1} |u_k\rangle. \tag{12}$$

The polarizability of the homogeneous particle is obtained by using the distribution (12) to build the solution (4) of the Laplace equation and use it in Eq. (2). It has been shown that, operationally, the polarizability is simply the dipole moment of the distribution (12) over unit volume [25,27]

$$\alpha = \frac{1}{3}\frac{1}{V_1}\sum_{i,k} \frac{\langle \mathbf{x}\cdot\mathbf{N}_i|u_k\rangle\langle v_k|\mathbf{n}\cdot\mathbf{N}_i\rangle}{1/(2\lambda) - \chi_k}, \tag{13}$$

where $\mathbf{N}_i$ are three mutually orthogonal unit vectors, and $i = 1,2,3$. The factor $[1/(2\lambda) - \chi_k]^{-1}$ is a generalized Clausius–Mosotti factor. Each dipole-active eigenmode contributes to α according to its weight $p_k = \frac{1}{3}\frac{1}{V_1}\Sigma_i \langle \mathbf{x}\cdot\mathbf{N}_i|u_k\rangle\langle v_k|\mathbf{n}\cdot\mathbf{N}_i\rangle$, which determines the strength of coupling between the uniform electric field and the k-th eigenmode and contains three components $P_{k,i} = \langle \mathbf{x}\cdot\mathbf{N_i}|u_k\rangle\langle v_k|\mathbf{n}\cdot\mathbf{N_i}\rangle / V_1$. Equation (13) shows a clear separation of the electric properties, which are included only in λ, from the geometric properties expressed by χ_k and p_k.

B. Shelled particles

The polarizability of an object covered by a thin shell with permittivity ε_S can be calculated in a similar fashion. The electric field is now generated by two single layer distributions, and boundary conditions are imposed twice, for Σ_1 and for Σ_2. The surface Σ_1 is the outer surface of the shell and Σ_2 is the interface separating the interior from the shell. The solution of the electric potential of a shelled particle in terms of single layer potentials has the form [28]

$$\Phi(\mathbf{x}) = -\mathbf{x}\cdot\mathbf{N} + \frac{1}{4\pi}\int_{\Sigma_1} \frac{\mu_1(\mathbf{y})}{|\mathbf{x}-\mathbf{y}|} d\Sigma(\mathbf{y}) + \frac{1}{4\pi}\int_{\Sigma_2} \frac{\mu_2(\mathbf{y})}{|\mathbf{x}-\mathbf{y}|} d\Sigma(\mathbf{y}), \tag{14}$$

where μ_1 and μ_2 are the densities defined on surface Σ_1 and Σ_2, respectively. Four integral operators M_{11}, M_{12}, M_{21}, and M_{22} are defined, depending on which surface are variables $\mathbf{x}$ and $\mathbf{y}$. For example M_{11} is defined when $\mathbf{x}$ and $\mathbf{y}$ are both on Σ_1, M_{12} is defined by $\mathbf{x}$ on Σ_1 and $\mathbf{y}$ on Σ_2, and so on. Thus,

$$M_{ij}[\mu_j] = \frac{1}{4\pi}\int_{\Sigma_j} \mu_j(\mathbf{y}) \frac{\mathbf{n}(\mathbf{x})\cdot(\mathbf{x}-\mathbf{y})}{|\mathbf{x}-\mathbf{y}|^3} d\Sigma(\mathbf{y}), \tag{15}$$

for $i,j = 1,2$. The equations obeyed by μ_1 and μ_2 are

$$\mu_1/(2\lambda_1) - M_{11}[\mu_1] - M_{12}[\mu_2] = \mathbf{n}\cdot\mathbf{N},$$

$$\mu_2/(2\lambda_2) - M_{21}[\mu_1] - M_{22}[\mu_2] = \mathbf{n}\cdot\mathbf{N}. \tag{16}$$

Here, the electric parameters are $\lambda_1 = (\varepsilon_S - \varepsilon_0)/(\varepsilon_S + \varepsilon_0)$ and $\lambda_2 = (\varepsilon_1 - \varepsilon_S)/(\varepsilon_1 + \varepsilon_S)$.

We further assume a confocal geometry, i.e., the surface Σ_1 is a slightly scaled version of Σ_2, with a scaling factor η close to unity. This assumption does not provide constant thickness for the shell, but our main results should remain at least qualitatively valid [3,6].

In the limit of very thin shells, and using the scaling properties of the operator M, one can show [25,27] that all four M operators are related to $M = M_{11}$

$$M_{12}[\mu] = \eta^{-3}(\mu/2 + M[\mu]),$$

$$M_{21}[\mu] = -\mu/2 + M[\mu],$$

$$M_{22}[\mu] = M[\mu]. \tag{17}$$

Equations (16) can then be arranged in a matrix form as

$$\begin{bmatrix} 1/(2\lambda_1) - M & (1/2 + M)/\eta^3 \\ -1/2 + M & 1/(2\lambda_2) - M \end{bmatrix} \begin{pmatrix} \mu_1 \\ \mu_2 \end{pmatrix} = \begin{pmatrix} \mathbf{n}\cdot\mathbf{N} \\ \mathbf{n}\cdot\mathbf{N} \end{pmatrix}. \tag{18}$$

By knowing the eigenvectors and the eigenvalues of M the charge densities μ_1 and μ_2 can be found by inverting the matrix in Eq. (18). For example, μ_1 is

$$\mu_1 = \sum_k \frac{\eta^3\left(\frac{1}{2\lambda_2} - \chi_k\right) + \left(\frac{1}{2} + \chi_k\right)}{\eta^3\left(\frac{1}{2\lambda_1} - \chi_k\right)\left(\frac{1}{2\lambda_2} - \chi_k\right) + \left(\frac{1}{2} + \chi_k\right)\left(\frac{1}{2} - \chi_k\right)} \times \langle v_k|\mathbf{n}\cdot\mathbf{N}\rangle |u_k\rangle. \tag{19}$$

The field generated by the two distributions μ_1 and μ_2 outside the particle is the same as the field generated by an equivalent single layer distribution

$$\mu_e = \sum_k \langle v_k|\mathbf{n}\cdot\mathbf{N}\rangle[1/(2\tilde{\lambda}_k)-\chi_k]^{-1}|u_k\rangle, \quad (20)$$

where $\tilde{\lambda}_k=(\tilde{\varepsilon}_k-\varepsilon_0)/(\tilde{\varepsilon}_k+\varepsilon_0)$ and the equivalent permittivity $\tilde{\varepsilon}_k$ is defined for each eigenmode as

$$\tilde{\varepsilon}_k = \varepsilon_S\left[1+\frac{\varepsilon_1-\varepsilon_S}{\varepsilon_S+\delta(1/2-\chi_k)\varepsilon_1+\delta(1/2+\chi_k)\epsilon_S}\right], \quad (21)$$

where $\delta=\eta^3-1\ll 1$. The distribution (20) is similar with the distribution (12) obtained for a homogeneous particle, except that λ has to be replaced for each mode with an equivalent quantity $\tilde{\lambda}_k$. Equation (21) can be applied recursively for a multishelled structure. The strict separation of electric and geometric properties is weakened in this case, because the shape-dependent eigenvalue χ_k appears now in the electric equivalent quantity $\tilde{\lambda}_k$.

The polarizability of the shelled particle is obtained by using the distribution (20) to build the solution (4) of the Laplace equation and use it in Eq. (2), to get

$$\alpha = \frac{1}{3}\frac{1}{V_1}\sum_{i,k}\frac{\langle\mathbf{x}\cdot\mathbf{N}_i|u_k\rangle\langle v_k|\mathbf{n}\cdot\mathbf{N}_i\rangle}{1/(2\tilde{\lambda}_k)-\chi_k}. \quad (22)$$

Equation (22) is obtained by replacing λ with $\tilde{\lambda}_k$ in Eq. (13). The parameter V_1 in Eq. (22) is the total volume of the cell (the core and the shells). In the limit of a dilute suspension of identical shelled particles, with a low volume fraction f, the effective permittivity (1) is

$$\varepsilon_{\text{sus}} = \varepsilon_0\left[1+f\sum_k p_k\frac{\tilde{\varepsilon}_k-\varepsilon_0}{(1/2+\chi_k)\varepsilon_0+(1/2-\chi_k)\tilde{\varepsilon}_k}\right]. \quad (23)$$

C. Debye relaxation expansion

In general, the effective permittivity ϵ_{sus} of a suspension of objects with m shells will have $m+1$ Debye relaxation terms for each dipole active eigenmode. The proof is recursive and is based on partial fraction expansion with respect to variable $i\omega$ of Eqs. (22) and (23), provided that the complex permittivity of various dielectric phases is $\epsilon=\varepsilon-i\sigma/(\omega\varepsilon_{vac})$ where $i=\sqrt{-1}$ and ε_{vac} is the permittivity of the free space (8.85×10^{-12} F/m). Thus the first Debye term comes out from Eq. (23) and the remaining m Debye terms result from Eq. (21) by the homogenization process described for shelled particles. Hence, a suspension of cells with m shells (and $m+1$ interfaces) has a dielectric spectrum containing a number of Debye terms equal to $m+1$ times the number of dipole-active eigenvalues.

The suspension effective permittivity ϵ_{sus} has the expansion

$$\epsilon_{\text{sus}} = \epsilon_{\text{f}} + \sum_{k,j}\Delta\varepsilon_{kj}/(1+i\omega T_{\text{kj}}), \quad (24)$$

where $\epsilon_{\text{f}}=\varepsilon_{\text{hf}}-i\sigma_{\text{lf}}/(\omega\varepsilon_{vac})$, ε_{hf} is the high-frequency permittivity, and σ_{lf} is the low-frequency conductivity; $\Delta\varepsilon_{kj}$ and T_{kj} are the dielectric decrement and the relaxation time of the kj Debye term, respectively; index k enumerates the dipole-active eigenmodes and index j enumerates interfaces.

Although the measurable bulk quantities in Eq. (24) are directly correlated with the microscopic (electric and shape) parameters, a solution of the inverse problem, which aims at obtaining the microscopic information nonintrusively, from the effective permittivity, is in general difficult, if not impossible for the general multishell structure. However, biological cell has a thin and almost nonconductive membrane, and several simplifications and approximations can be made. Two Debye relaxation terms in the effective permittivity ϵ_{sus} are expected for each dipole-active eigenmode, corresponding to the two interfaces which define the membrane.

The first relaxation is derived from the equivalent permittivity [Eq. (21)], which can be written also as Debye relaxation terms,

$$\tilde{\epsilon}_k = \varepsilon + \Delta\varepsilon/(1+i\omega T). \quad (25)$$

The relaxation time T that is given by the poles of $\tilde{\epsilon}_k$ in Eq. (21) is a quite good approximation of the first relaxation time T_{k1},

$$T = \varepsilon_{vac}\frac{(1+\delta/2+\delta\chi_k)\varepsilon_S+\delta(1/2-\chi_k)\varepsilon_1}{(1+\delta/2+\delta\chi_k)\sigma_S+\delta(1/2-\chi_k)\sigma_1} \approx T_{k1}. \quad (26)$$

The main reason is as follows: at frequencies close to $1/T$ there is a huge change in $\tilde{\epsilon}_k$ of order $\varepsilon_S/[\delta(1/2-\chi_k)]$, and consequently a significant change in the total permittivity ϵ_{sus} given by Eq. (23). Therefore, T provides an approximate value for the relaxation time T_{k1} of the suspension effective permittivity ϵ_{sus}.

For a non-conductive shell $\sigma_S\approx 0$, or more precisely when $\sigma_S\ll\delta(1/2-\chi_k)\sigma_1$, the relaxation time [Eq. (26)] is

$$T_{k1} \approx \frac{\varepsilon_{vac}\varepsilon_S}{\delta\cdot\sigma_1(1/2-\chi_k)}, \quad (27)$$

showing a strong dependence on the thickness of the shell and on the shape of the particle, through the eigenvalue χ_k. Due to the small parameter δ in Eq. (27) the first relaxation (i.e., membrane relaxation) tends to have a lower frequency than the second relaxation, which is present even for particles with no shell (see the discussion below). In addition, cumbersome but straightforward calculations provide the dielectric decrement $\Delta\varepsilon_{k1}$ in Eq. (24)

$$\Delta\varepsilon_{k1} \approx \frac{fp_k\varepsilon_S}{\delta(1/2+\chi_k)^2(1/2-\chi_k)}, \quad (28)$$

that is very large due to the same strong dependence on the thickness of the shell. The effect is even more dramatic when the second largest eigenvalue is very close to the largest eigenvalue, $(1/2-\chi_2)\to 0$, like in the case of two cells connected by tight junctions.

For a suspension of shelled spheres $\eta=1+\Delta R/R$ and $\delta=\eta^3-1\approx 3\Delta R/R$, where ΔR is the thickness of the membrane, R is inner radius, and $R+\Delta R$ is the total radius. Thus, both T_{k1} and $\Delta\varepsilon_{k1}$ are proportional to R and ε_S and inversely proportional to ΔR in accord to the Pauly–Schwan theory [1,8]. Moreover, the dielectric decrement $\Delta\varepsilon_{k1}$ in Eq. (28) is a generalization of Eq. (54a) in [8]. In the same time, the relaxation time [Eq. (27)] differs with respect to Eq. (56a) in [8]. only by the conductivity term. We will show elsewhere

that a more appropriate treatment of the relaxation times recovers also the relaxation time given by Eq. (54a) in [8].

Thus, a nonconductive and thin shell/membrane produces a large relaxation of the complex permittivity of the suspension [31]. The experimental evidences further support these theoretical facts, when attacking the membrane with a membrane disrupting compound (for example a detergent) the relaxation almost vanishes as the cellular membrane is permeated [32].

For frequencies higher than $1/T_{k1}$ the cell permittivity is essentially determined by the dielectric properties of the cytoplasm, and does not depend on membrane's properties. The second Debye relaxation occurs at higher frequencies than the first (membrane) relaxation, and has the relaxation time,

$$T_{k2} \approx \varepsilon_{vac} \frac{(1/2+\chi_k)\varepsilon_0 + (1/2-\chi_k)\varepsilon_1}{(1/2+\chi_k)\sigma_0 + (1/2-\chi_k)\sigma_1}, \tag{29}$$

derived from the pole of Eq. (23). The corresponding dielectric decrement is

$$\Delta\varepsilon_{k2} \approx fp_k(1/2-\chi_k)(\varepsilon_1\sigma_0 - \varepsilon_0\sigma_1)^2 \times ((1/2+\chi_k)\varepsilon_0 + (1/2-\chi_k)\varepsilon_1)^{-1} \times ((1/2+\chi_k)\sigma_0 + (1/2-\chi_k)\sigma_1)^{-2},$$

The last two equations are similar to the ones that are given for spherical particles in [8] [Eqs. (46) and (49) in the aforementioned reference]. The relaxation given by T_{k2} is basically the relaxation of a homogenous particle embedded in a dielectric environment and was also discussed in [22] by a closely related spectral method. If the conductivity of the cytoplasm is comparable to the conductivity of the outer medium, the decrement of the second relaxation is small such that it cannot be distinguished in the spectrum. On the contrary, if the conductivity of the outer medium is much greater or smaller that of cytoplasm, than a second observable relaxation occurs. Unlike the membrane relaxation, this second relaxation depends only weakly on the shape. By assuming that $\sigma_0 \ll \sigma_1$ and by using a finite-difference method, this resonance was also obtained in [3] and it was instrumental in explaining the experimental data on the fission of yeast cells of Asami *et al.* [33] by Lei *et al.* [22].

The shape of the particle is important because it affects the number of dipole-active eigenvalues and their strengths. In principle, each dipole-active eigenvalue introduces a new relaxation in the dielectric spectrum, providing this relaxation is well separated from the others. A cluster with complex geometry can have several dipole-active eigenvalues, but unless the cluster is larger in one dimension then in the others, or there are tight junctions, the relaxations overlap to create broad features in the spectrum. An extra relaxation is introduced when the particles are covered by thin membranes. In addition, if $(1/2-\chi_k) \to 0$ for that eigenvalue, then the shell induced relaxation has low frequency, large relaxation time, and large dielectric decrement. Based on the spectral BIE method, it is therefore possible to explicitly relate the dielectric spectra of cell suspensions to cell's geometry and electric parameters, and, even design fitting procedures to evaluate these parameters from measurements.

III. RESULTS

A. Numerical procedure

The calculation of the effective permittivity for a suspension uses Eq. (1) or Eq. (23), and reduces then to finding the eigenvalues χ_k and eigenvectors $|u_k\rangle$ and $|v_k\rangle$ of the linear response operator M. This problem is solved by employing a finite basis of NB functions defined on the surface Σ. A natural basis for a surface not far from a sphere is the generalized hyperspherical harmonics functions,

$$\tilde{Y}_{lm}(\mathbf{x}) = \frac{1}{\sqrt{s(\mathbf{x})}} Y_{lm}[\theta(\mathbf{x}), \varphi(\mathbf{x})], \tag{30}$$

where $s(\mathbf{x})$ is related to the surface element through $d\Sigma = s(\mathbf{x}) d\Omega_{\mathbf{x}}$ and $d\Omega_{\mathbf{x}}$ is the solid angle element.

Another choice could be based on Chebyshev polynomials of the first kind [29]

$$\tilde{T}_{lm}(\mathbf{x}) = \frac{1}{\sqrt{s(\mathbf{x})}} T_l[\theta(\mathbf{x})] e^{im\varphi(\mathbf{x})}. \tag{31}$$

Both bases are complete and orthogonal in the Hilbert space of square integrable functions defined on Σ.

In this paper, we model the linear cluster of particles as an object with axial symmetry. We seek to find a surface of revolution for which the thickness of the interparticle joints can be varied without perturbing the overall shape of the object. We use two representations for the surface Σ: (A) for clusters of two particles we use spherical coordinates $\{x,y,z\} = \{r(\theta)\sin\theta\cos\phi, r(\theta)\sin\theta\sin\phi, r(\theta)\cos\theta\}$, and (B) for clusters with more than two particles we specify the surface in terms of a function $g(z)$ as $\{x,y,z\} = \{g(z)\cos\phi, g(z)\sin\phi, z\}$.

In the case B, the surface element is

$$d\Sigma = g(z)\sqrt{1+g'^2(z)}\, dz d\varphi, \tag{32}$$

and the normal to surface Σ is

$$\mathbf{n} = \frac{1}{\sqrt{1+g'^2(z)}} \begin{bmatrix} \cos\varphi \\ \sin\varphi \\ -g'(z) \end{bmatrix}. \tag{33}$$

In the basis of generalized hyperspherical harmonics the operator M has matrix elements given by

$$M_{lm;l'm'} = \delta_{mm'} \int \int_0^{2\pi} \int \int_{z_{\min}}^{z_{\max}} A(z,z',\varphi-\varphi') P_l^m \times [\cos\theta(z)] P_{l'}^{m'} [\cos\theta(z')] e^{im(\varphi-\varphi')} \times G(z,z') dz dz' d\varphi d\varphi', \tag{34}$$

where

$$G(z,z') = \sqrt{g(z)g(z')\sqrt{[1+g'(z)][1+g'(z')]^{-1}}}, \tag{35}$$

and

$$A(z,z',\phi) = \frac{[g(z)-g(z')]\cos\phi - (z-z')g'(z)}{[g^2(z)+g^2(z')-2g(z)g(z')\cos\phi+(z-z')^2]^{3/2}}. \tag{36}$$

After the angle integration in Eq. (34) and by using the elliptic integrals given in the Appendix, the matrix elements are obtained by numerical evaluation of the resulting (z,z') double integral using an NQ-point Gauss–Legendre quadrature [29,30]. Because of the integrable singularity apparent in the kernel of the operator M in Eq. (6), the mesh of z must be shifted from the mesh of z' by a transformation which insures that there is no overlap between the two meshes.

The delta symbols $\delta_{mm'}$ in Eq. (34) reflects the fact that we consider only objects with rotational symmetry in this paper. Moreover, for fields parallel with the cluster axis $m=0$, while $m=1$ for perpendicular fields.

The convergence of the results is obtained in two steps. First, the number NQ of quadrature points is increased until the matrix elements of M converge, and then the size NB of the basis set is increased until the relevant eigenvalues χ_k and their corresponding weights p_k have acquired the desired accuracy. A necessary test for convergence is the fulfillment of the sum rules $\Sigma_k P_{k,i}=1$ and $\Sigma_{i,k}\chi_k P_{k,i}=1/2$ with sufficient accuracy [18,19]. Usually the convergence is fast in both the number of quadrature points and the size of basis, unless the system has a tight junction where some care must be considered in order to achieve the required accuracy of the eigenmodes with the eigenvalues close to 1/2. For a sphere there is just one dipole-active eigenmode which has eigenvalue $\chi=1/6$ and weight $p=1$, while for an ellipsoid there is one dipole-active eigenmode along each axis. Fast and accurate solutions are achieved for spheroids with a basis size of $NB=20$ and with $NQ=64$ quadrature points. In general, the size of the basis and the number of the quadrature points increase with the number of cells in the cluster and with the decreasing of the junction size. Thus, for our numerical examples a basis with $NB=35-40$ and $NQ=128$ quadrature points are enough for a converged solution in the case of the dimers and $NB=50$ and $NQ=200$ quadrature points in the case of the clusters with up to four cells.

B. Two cells joined by tight junction

The equation $r(\theta)=(h+\cos^2\theta)/(1-a\cos^2\theta)$ describes the shape of a two-particle cluster. Parameter h controls the tightness of the interparticle junction and parameter a measures the deviation from a spherical shape. More precisely, h is the radius of the smallest circle at around the thinnest part of the junction.

Figure 1 shows the effective permittivity for a suspension of particles with the following parameters: $\varepsilon_1=70$, $\sigma_1=0.25$ S/m, $\varepsilon_S=6$, $\sigma_S=0$, $\varepsilon_0=81$, $\sigma_0=0.374$ S/m, volume fraction $f=0.05$, membrane thickness $\delta=0.00947275$ and $a=0.2$. The effective permittivity does not depend on the thickness parameter h when the stimulus electric field is perpendicular to the cluster axis. However, a new relaxation becomes apparent as $h\to 0$, for parallel fields [3,25].

Figure 2 presents the first 7 eigenvalues χ_k and their weights $P_{k,1}$ for a field parallel to the z axis. As the junction become tighter $(h\to 0)$ more eigenvalues become dipole-active. While all eigenvalues are important in shaping the dielectric spectrum, the second largest eigenvalue χ_2 is crucial to explaining the occurrence of an additional relaxation at low frequencies, as observed for small h in [3,25]. Although its weight $P_{2,1}$ also decreases for small h, this dipole

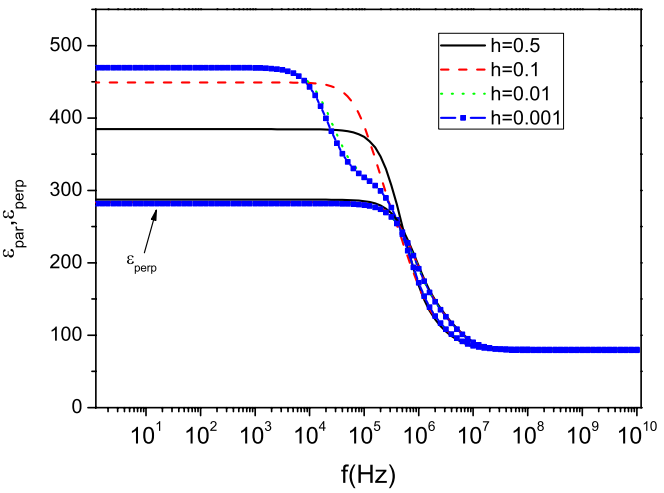

FIG. 1. (Color online) The spectrum of the effective permittivity of a suspension of dimers with various junction thickness h, and with parallel and perpendicular field configurations. The suspension permittivity for an electric field perpendicular to cluster axis does not depend on h and is pointed by an arrow.

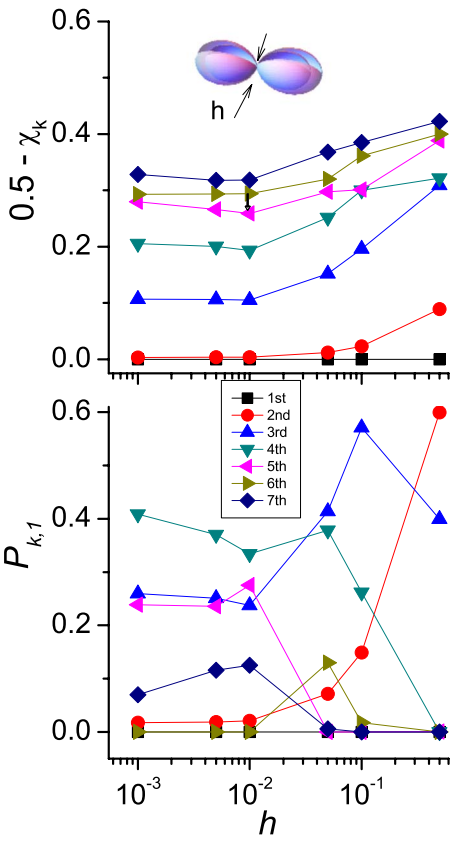

FIG. 2. (Color online) The largest seven eigenvalues and their weights for a binary cluster with parameter $a=0.2$, as a function of h. The inset shows the shape of the dimer.

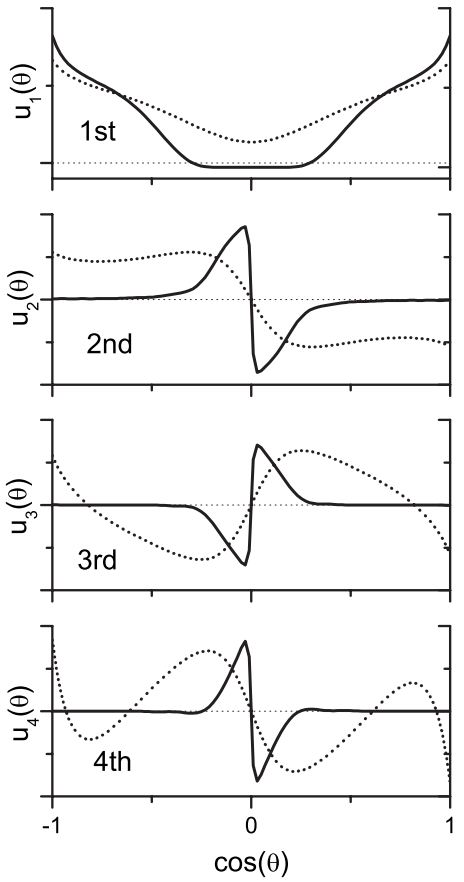

FIG. 3. The first four eigenvectors for a dimer given by equation $r(\theta)$; $a=0.2$ and $h=0.5$ (dotted line) and $h=0.01$ (solid line).

active eigenmode approaches 1/2 as the junction becomes tighter. Thus, according to Eqs. (27) and (28) the effect of χ_2 is "enhanced" due to the presence of a nonconductive shell (as the case for biological particles analyzed in [3,25]). Moreover, the decrease in $P_{2,1}$ is compensated by the increase of $1/(1/2-\chi_2)$.

The presence of a new relaxation at low frequency along with its relationship with the size of h has been already singled out in Gheorghiu *et al.* [25] by using the same method but without the analysis of dipole-active eigenmodes. Using a finite discrete model [3], the relaxation was observed before the segregation during cell division, while other papers [34,35] fail to relate the size of h to the new relaxation, even though one of them [34] employs essentially the same method as the one outlined in the present work.

Figure 3 shows the charge distribution associated with the first four eigenvalues for two distinct values of h. The second eigenmode is an antisymmetric combination of net charge

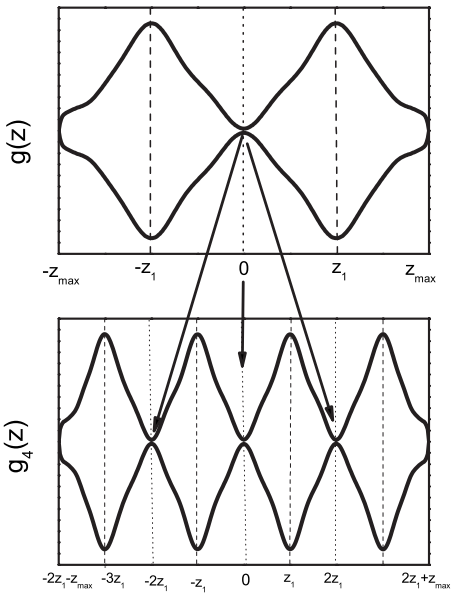

FIG. 4. Smooth construction of a cluster (lower panel) from a dimer (upper panel). The parts determined by $z\in[-z_1,z_1]$ are "glued" together with the ends of the dimer. The arrows show where the junctions will be placed in the cluster.

distributions (monopoles) on each particle of the dimer. The third charge distribution is an antisymmetric combination of charge distributions with a dipole moment on each part of the dimer and the forth distribution is antisymmetric combination of charge distributions with a quadrupole moment on each particle. At small h (tight junctions), charge accumulates in the vicinity of the junction [36].

C. Clusters of more than two particles

Smoother yet tight junctions would bring $(1/2-\chi_2)$ closer to 0 than sharp and tight junctions. The reason is simple: smoother junctions have the two parts of the dimer farther apart. We have analyzed linear clusters of cells connected by smooth and tight junctions by using a (z,ϕ) parameterization, which describes a surface by $\{x=g(z)\cos\varphi, y=g(z)\sin\varphi, z\}$. The construction starts from a dimer shape that resembles the shape of the epithelial cells such as Madin–Darby canine kidney (MDCK) cells. An example of such shape, displayed in Fig. 4, extends from $-z_{\max}$ to $z_{\max}$ and it can be decomposed in three parts, the left cap ($-z_{\max}\le z\le -z_1$), the central part ($-z_1\le z\le z_1$), and the right cap ($z_1\le z\le z_{\max}$). At position $\pm z_1$ the shape function has its maximum. An m-cell linear cluster is obtained by repeating the central part $m-1$ times and it extends from $-L_m$ to L_m, where $L_m=z_{\max}+(m-2)z_1$. Mathematically, the shape is described by:

$$g_m(z)=\begin{cases} g[z+(m-2)z_1], & \text{for } -L_m\le z\le -L_m+z_{\max} \\ g(\mathrm{mod}\{z+[1+(-1)^m]z_1/2,2z_1\}-z_1), & \text{for } -L_m+z_{\max}\le z\le L_m-z_{\max} \\ g[z-(m-2)z_1], & \text{for } L_m\le z\le L_m-z_{\max}, \end{cases} \tag{37}$$

TABLE I. Most representative dipole-active eigenmodes and their weights for the trimer in parallel field.

χ_k	$P_{k,1}$
0.4996	0.01305
0.40642	0.07769
0.40448	0.1391
0.37763	0.17366
0.26409	0.20519
0.23809	0.01839
0.17557	0.05104
0.13522	0.05234
0.12165	0.01066
0.07192	0.06197
0.06649	0.01239
0.03479	0.03899
0.03362	0.02823
0.0281	0.04688
0.02377	0.02519

where $\mathrm{mod}(x,y)$ is the remainder of the division of x by y. For the examples considered here, the dimer shape function is:

$$g(z) = 0.01 + 2.32317z^2 - 11.9862z^4 + 40.4045z^6 - 74.2226z^8 + 79.142z^{10} - 51.8929z^{12} + 21.3096z^{14} - 5.35113z^{16} + 0.752147z^{18} - 0.045375z^{20}, \quad (38)$$

with $z_{\max}=1.77377$ and $z_1=z_{\max}/2$.

Tables I and II list the most representative dipole-active eigenmodes for a trimer in perpendicular and parallel fields. Only the parallel field configuration has a dipole-active eigenvalue close to 1/2, with a relatively small weight.

The results for linear clusters of up to four particles are displayed in Fig. 5. The electric parameters are the same as ones used for dimers in the previous section. An additional, distinct low-frequency relaxation emerges for clusters with more then one particles, only when the stimulus field is parallel with the symmetry axis. The relaxation frequency

TABLE II. Most representative dipole-active eigenmodes and their weights for the trimer in perpendicular field.

χ_k	$P_{k,2}$
0.1831	0.64102
0.06964	0.01464
0.05492	0.01343
0.0272	0.01065
0.01674	0.05687
0.01479	0.13179
0.00395	0.05029
−0.01635	0.03246

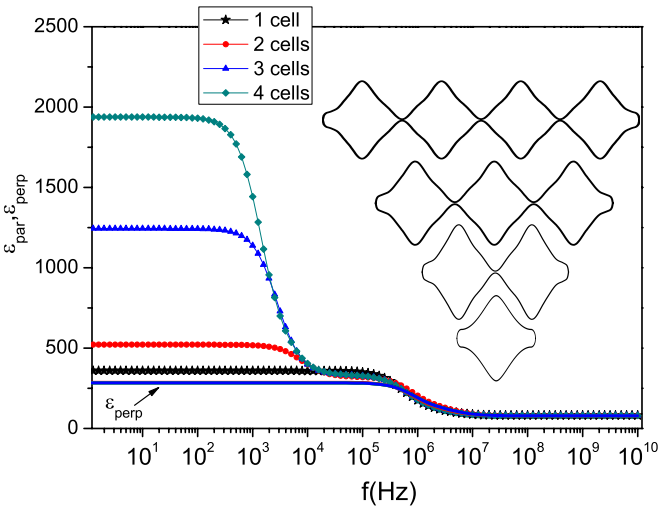

FIG. 5. (Color online) Effective permittivity for clusters (shown in the inset) of one, two, three, and four cells connected by tight and smooth junctions. The field is either parallel (solid lines with symbols) or perpendicular (solid lines only) to the cluster axis. The effective permittivity either increases strongly with the number of cells for parallel geometry, or does not change for a perpendicular geometry.

decreases, while the intensity of these relaxations increases, as the number of cluster members increases. This behavior is explained again by the combination of eigenvalues close to 1/2, with thin nonconductive layers covering the cluster and is consistent with experimental data on ischemic tissues [11], which reports that the cell separation (closure of gap junctions) is responsible for decrease and eventual disappearance of the low-frequency dispersion.

In Fig. 6 we plot $P_{k,1}/(1/2-\chi_k)$ versus $(1/2-\chi_k)$, which shows that the number of dipole-active eigenmodes increases with the number of particles in the cluster. According to Eqs. (27) and (28), Fig. 6 shows in fact the dielectric decrement versus its corresponding relaxation frequency for each dipole-active eigenmode of the given clusters. For clusters of two or three particles, there is one important active eigenmode close to 1/2, while for clusters of four particles there are two active eigenmodes.

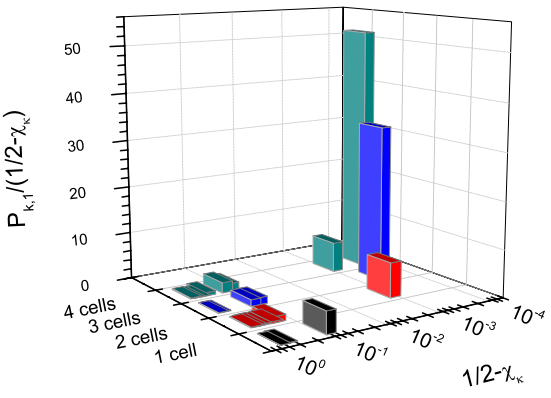

FIG. 6. (Color online) $P_{k,1}/(1/2-\chi_k)$ versus $(1/2-\chi_k)$ for clusters of up to four cells. The second eigenvalue has the largest contribution to intensity of relaxation.

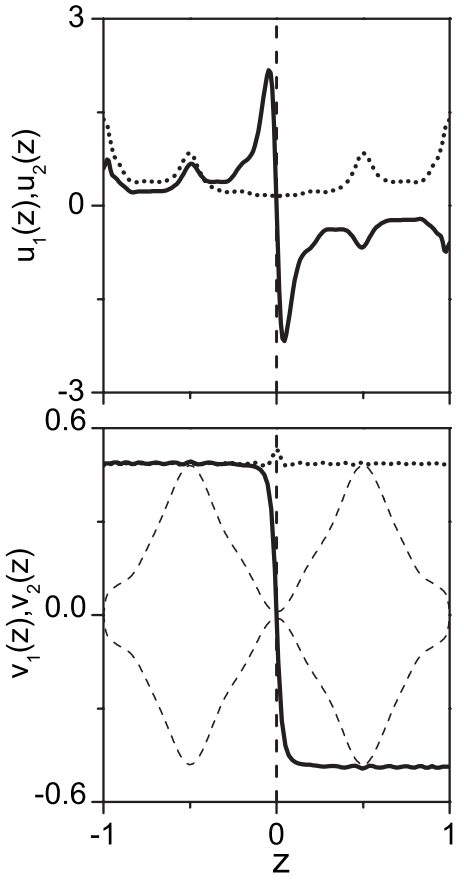

FIG. 7. The first (dotted line) and the second (solid line) eigenfunction of M (upper panel) and $M^{\dagger}$ (lower panel) for a dimer whose shape is depicted by dashed line in the lower panel. The second eigenfunction of $M^{\dagger}$ is an antisymmetric combination of almost constant distributions on each part of the dimer.

It can be conjectured that for a general linear cluster made of m particles, there are $m-1$ eigenvalues close to 1/2, of which the largest one is always dipole-active and has the largest weight. In fact one can show that for two cells connected by smooth and tight junction characterized by parameter h, $(1/2-\chi_2)\propto h^2$ when $h\to 0$, or more precisely $(1/2-\chi_2)$ is proportional with the solid angle encompassed by the missing part of a cell when it is connected with other cell in the dimer. The proof is based on the theorem of the solid angle [12]. The generalization to a finite cluster is also straightforward to $(1/2-\chi_2)\propto h^2/m$ (in that case the solid angle encompassed by the middle junction is proportional to h^2/m. The weight of the second eigenmode is $P_{2,1}=\langle \mathbf{x}\cdot\mathbf{N_1}|u_2\rangle\langle v_2|\mathbf{n}\cdot\mathbf{N_1}\rangle/V_1$. If we consider that the surface of the cluster is determined by the function $g(z)$ then, up to a constant factor, $\langle v_2|\mathbf{n}\cdot\mathbf{N_1}\rangle\approx g(0)^2=h^2$ for two cells connected by smooth and tight junctions. The proof considers that the second eigenfunction of $M^{\dagger}$ is an antisymmetric combination of constant distributions on each part of the dimer. This assertion is confirmed in Fig. 7. Moreover, $\langle \mathbf{x}\cdot\mathbf{N}_1|u_2\rangle/V_1$ is weakly dependent on h. Therefore, for a parallel setting of the field stimulus, $P_{2,1}/(1/2-\chi_2)$, which is the measure of the dielectric decrement of low-frequency relaxation, is finite and it increases when the number of cells is increased. The increase of relaxation decrement when $m\to\infty$ is physically limited by $\sigma_S \ll \delta(1/2-\chi_k)\sigma_1$, since the membrane conductivity is not strictly 0.

Due to cluster's shape and membrane properties, the variation of $P_{k,1}/(1/2-\chi_k)$ and $(1/2-\chi_k)$ with respect the eigenmode k determines a low-frequency relaxation when the dipole-active eigenvalue χ_k is close to 1/2. We note here that for dipole-active eigenmodes of ellipsoids the term $(1/2-\chi_k)$ is called the depolarization factor and has analytical expression [37]. Prolate spheroids with longitudinal axis much larger than the transverse axis (needles) have the longitudinal depolarization factor approaching 0 and the transverse depolarization factor approaching 1/2. More precisely, for a long prolate spheroid, the longitudinal depolarization factor scales as $(1/2-\chi_2)\propto a_x^2/a_z^2$, $a_z>a_x=a_y$, as $a_x\to 0$. On the other hand, extensive numerical calculations support the fact that cylinders with the same aspect ratio behave similarly to prolate spheroids [37]. Thus, it is not hard to observe that the low-frequency relaxation of linear clusters of cells connected by tight junctions is similar to that of a needle or a thin cylinder as long as the cluster and as thick as the junction. On the other hand, the high-frequency relaxation of the cluster shows the relaxation of a suspension of spheroids with the same volume as the volume of a single cell. Therefore, the dielectric spectrum for a suspension of clusters is the same as the spectrum of a two species suspension made of thin cylinders and spheroids.

IV. CONCLUSIONS

We present a theoretical framework based on a spectral representation of BIE and able to calculate the dielectric behavior of linear clusters with a wide range of shapes and dielectric structures. The theory agrees with the results of Pauly and Schwan for a sphere covered with a shell [1,8]. In fact, for spheroids, our theory is the same as the analytical results of Asami *et al.* [2]. We present extensive calculations of clusters with shapes resembling MDCK cells.

A practical numerical recipe to compute the effective permittivity of linear clusters with arbitrary number of cells is provided. Examples are given for clusters with shapes described as $r(\theta)$ in spherical coordinates or using (z,φ) parameters as $\{x=g(z)\cos\varphi, y=g(z)\sin\varphi, z\}$. Other studies in the literature used only spherical coordinates representation [25,27,35]. A direct relation between the geometry and dielectric parameters of the cells and their dielectric behavior described by a Debye representation has been formulated for the first time. Other work [22], which is based on a closely related spectral method [18–21], found a direct relation linking the geometry and electric parameters to the dielectric behavior only for homogenous particles. Moreover, the method used in [22] treats only particles with spheroidal geometry.

We show that the spectral representation provides a straightforward evaluation of the characteristic time constants and dielectric decrements of the relaxations induced by cell membrane. We prove that the effective permittivity is sensitive to the shape of the embedded particles, specially when the linear response operator has strong dipole active

modes (with large weights p_k). A low-frequency and distinct relaxation occurs when the largest dipole-active eigenvalue is very close to 1/2. Clusters of living cells connected by tight junctions or very long cells have such an eigenvalue. Our results also shed a new light on the understanding of recent numerical calculations [38] performed with a boundary element method on clustered cells where the low-frequency relaxation is attributed to the tight (gap) junctions connecting the cells. The method used in [38] does not use the confocal geometry assumption.

The present work has several implications and applications. We emphasize the capabilities of dielectric spectroscopy to monitor the dynamics of cellular systems, e.g., cells during cell cycle division, using synchronized yeast cells [3,11,39], or monolayers of interconnected cells [40,41]. Also the method is able to assess the dielectric behavior of linear aggregates or rouleaux of erythrocytes, where the ellipsoidal or cylindrical approximations are not adequate [42,43].

The proposed representation is a powerful alternative to finite element or other purely numerical approaches, because it provides the analytical framework to explain and predict the complex dielectric spectra occurring in bioengineering applications. Extension of this method to other surfaces of revolution, for example linear clusters with more than 4 particles, is straightforward providing an adequate parametric equation is available. Finally, in many cases (e.g., shapes with high symmetry) the method is faster, offers accurate solutions and last but not least can be integrated in fitting procedures to analyze experimental spectra.

ACKNOWLEDGMENTS

This work has been supported by Romanian Project "Ideas" (Grants No. 120/2007 and No. FP 7) and Nanomagma (Grant No. 214107/2008).

APPENDIX: INTEGRATION OVER φ

The integrals over $(\varphi-\varphi')$ are performed with the following elliptic integrals,

$$\int_0^\pi \frac{1}{(a-b\cos\varphi)^{3/2}}d\varphi = \frac{2}{\sqrt{a-b}}\frac{1}{a+b}E\left(-\frac{2b}{a-b}\right) \tag{A1}$$

$$\int_0^\pi \frac{\cos\varphi}{(a-b\cos\varphi)^{3/2}}d\varphi = \frac{2}{\sqrt{a-b}}\frac{1}{b}\left[\frac{a}{a+b}E\left(-\frac{2b}{a-b}\right) - K\left(-\frac{2b}{a-b}\right)\right], \tag{A2}$$

$$\int_0^\pi \frac{\cos^2\varphi}{(a-b\cos\varphi)^{3/2}}d\varphi = \frac{2}{\sqrt{a-b}}\frac{1}{b^2}\left[\frac{2a^2-b^2}{a+b}E\left(-\frac{2b}{a-b}\right) - 2aK\left(-\frac{2b}{a-b}\right)\right], \tag{A3}$$

where $K(x)$ and $E(x)$ are the complete integrals of the first and second kind, respectively [29].

[1] H. Pauly and H. P. Schwan, Z. Naturforsch. B **14**, 125 (1959).
[2] K. Asami, T. Hanai, and N. Koizumi, Jpn. J. Appl. Phys. **19**, 359 (1980).
[3] K. Asami, J. Phys. D **39**, 492 (2006).
[4] E. Fear and M. Stuchly, IEEE Trans. Biomed. Eng. **45**, 1259 (1998).
[5] K. Sekine, Y. Watanabe, S. Hara, and K. Asami, Biochim. Biophys. Acta **1721**, 130 (2005).
[6] M. Sancho, G. Martinez, and C. Martin, J. Electrost. **57**, 143 (2003).
[7] C. Brosseau and A. Beroual, Prog. Mater. Sci. **48**, 373 (2003).
[8] H. P. Schwan and K. R. Foster, in *Handbook of Biological Effects of Electromagnetic Fields*, edited by C. Polk and E. Postow (CRC, Boca Raton, Florida, 1996), p. 25.
[9] E. Gheorghiu, Phys. Med. Biol. **38**, 979 (1993).
[10] E. Gheorghiu, J. Phys. A **27**, 3883 (1994).
[11] J. Knapp, W. Gross, M. M. Gebhard, and M. Schaefer, Bioelectrochemistry **67**, 67 (2005).
[12] V. S. Vladimirov, *Equations of Mathematical Physics* (MIR, Moscow, 1984).
[13] F. Ouyang and M. Isaacson, Philos. Mag. B **60**, 481 (1989).
[14] D. R. Fredkin and I. D. Mayergoyz, Phys. Rev. Lett. **91**, 253902 (2003).
[15] I. D. Mayergoyz, D. R. Fredkin, and Z. Zhang, Phys. Rev. B **72**, 155412 (2005).
[16] D. Vrinceanu and E. Gheorghiu, Bioelectrochem. Bioenerg. **40**, 167 (1996).
[17] T. Hanai, H. Z. Zhang, K. Sekine, K. Asaka, and K. Asami, Ferroelectrics **86**, 191 (1988).
[18] D. J. Bergman, Phys. Rep. **43**, 377 (1978).
[19] D. J. Bergman and D. Stroud, in *Solid State Physics*, Vol. 46, edited by H. Ehrenreich and D. Turnbull (Academic, New York, 1992), p. 147.
[20] M. I. Stockman, S. V. Faleev, and D. J. Bergman, Phys. Rev. Lett. **87**, 167401 (2001).
[21] K. Li, M. I. Stockman, and D. J. Bergman, Phys. Rev. Lett. **91**, 227402 (2003).
[22] J. Lei, J. T. K. Wan, K. W. Yu, and H. Sun, Phys. Rev. E **64**, 012903 (2001).
[23] J. P. Huang, K. W. Yu, and G. Q. Gu, Phys. Rev. E **65**, 021401 (2002).
[24] K. Asami, E. Gheorghiu, and T. Yonezawa, Biochim. Biophys. Acta **1381**, 234 (1998).
[25] E. Gheorghiu, C. Balut, and M. Gheorghiu, Phys. Med. Biol. **47**, 341 (2002).
[26] J. D. Jackson, *Classical Electrodynamics*, 2nd ed. (Wiley, New York, 1975).
[27] C. Prodan and E. Prodan, J. Phys. D **32**, 335 (1999).
[28] J. L. Sebastián, S. Muñoz, M. Sancho, and G. Álvarez, Phys. Rev. E **78**, 051905 (2008).

[29] *Handbook of Mathematical Functions with Formulas, Graphs, and Mathematical Tables*, 9th ed., edited by M. Abramowitz and I. Stegun (Dover, New York, 1972).
[30] J. P. Boyd, *Chebyshev and Fourier Spectral Methods* (Dover, New York, 2001).
[31] H. Fricke, J. Appl. Phys. **24**, 644 (1953).
[32] K. Asami, T. Hanai, and N. Koizumi, J. Membr. Biol. **34**, 145 (1977).
[33] K. Asami, Biochim. Biophys. Acta **1472**, 137 (1999).
[34] A. Di Biasio and C. Cametti, Biolectrochemistry **71**, 149 (2007).
[35] A. Di Biasio, L. Ambrosone, and C. Cametti, J. Phys. D **42**, 025401 (2009).
[36] V. V. Klimov and D. V. Guzatov, Phys. Rev. B **75**, 024303 (2007).
[37] J. Venermo and A. Sihvola, J. Electrost. **63**, 101 (2005).
[38] A. Ron, N. Fishelson, N. Croitoriu, D. Benayahu, and Y. Shacham-Diamand, Biophys. Chem. **140**, 39 (2009).
[39] E. Gheorghiu and K. Asami, Bioelectrochem. Bioenerg. **45**, 139 (1998).
[40] J. Wegener, C. R. Keese, and I. Giaever, Exp. Cell Res. **259**, 158 (2000).
[41] E. Urdapilleta, M. Bellotti, and F. J. Bonetto, Phys. Rev. E **74**, 041908 (2006).
[42] J. L. Sebastián, S. Muñoz San Martín, M. Sancho, J. M. Miranda, and G. Álvarez, Phys. Rev. E **72**, 031913 (2005).
[43] K. Asami and K. Sekine, J. Phys. D **40**, 2197 (2007).